

Statistical Virtual Temperature of Classical and Quantum Systems

Tariq Aziz¹, Meng-Long Song¹, Liu Ye¹, Dong Wang^{1,*}, José J. Gil^{2,*}, and Sabre Kais³

¹*School of Physics and Optoelectronic Engineering, Anhui University, Hefei 230601, China*

²*Photonic Technologies Group, University of Zaragoza, Pedro Cerbuna 12, 50009 Zaragoza, Spain*

³*Department of Electrical and Computer Engineering, North Carolina State University, Raleigh, NC 27606, USA*

*Corresponding author emails:

dwang@ahu.edu.cn

ppgil@unizar.es

Abstract

In this work, we introduce a foundational definition of statistical virtual temperature, derived from the spectrum of the Gibbs Kubo-Martin-Schwinger (KMS) state and formulated using $d-1$ indices of purity (IP), where d represents the Hilbert space dimension within the C*-algebra framework. We demonstrate that the universal physical bounds between von Neumann entropy and statistical virtual temperature are constrained by these IPs, which may offer broader applications to quantum systems. Additionally, we geometrize classical optical polarization states of an arbitrary electromagnetic field and provide an interpretation of the quantum Mpemba effect, where a quantum system prepared at a higher statistical virtual temperature relaxes to equilibrium faster than one at a lower temperature. This behavior is explained through a novel concept of temperature-resolved entanglement asymmetry. Additionally, we present a geometric interpretation of the third law of thermodynamics using these entropy-temperature diagrams. Nevertheless, the defined statistical virtual temperature inherently exhibits the third law of thermodynamics. We believe that this work has the potential to significantly advance our understanding of classical polarization theory, quantum information theory, and quantum thermodynamics, and it may establish new connections and insights into these fields.

The concept of temperature at the nanoscale has undergone significant evolution across various studies in physics¹⁻³. Several authors have presented the idea of virtual temperature to understand the fundamental role of temperature in understanding both classical and quantum systems⁴⁻¹³. Brosseau and Bicoût⁵ introduced the concept of an effective polarization temperature in their study of entropy production due to the multiple scattering of light by a spatially random medium composed of uncorrelated spherical dielectric particles. They proposed that multiple scattering can be viewed as an order-disorder transition. They drew an analogy between the two-dimensional degree of polarization of light and the entropy of an Ising spin chain in contact with a heat bath. The Hamiltonian for the nearest neighboring spins $\sigma_i = \pm 1$ interacting with the exchange energy J in the absence of an external magnetic was defined as $-J \sum_{i,j=1}^N \sigma_i \sigma_j$. The entropy S for Ising spin chain with N numbers of atoms was

$$\frac{S(J\beta)}{Nk_B} = \log[2 \cosh(J\beta)] - J\beta \tanh(J\beta), \quad [1]$$

where k_B is the Boltzmann constant and β is the inverse temperature. This expression was compared with the two-dimensional von Neumann entropy and the expression for the polarization temperature τ for the plane wave with degree of polarization P_1 using the relation $\frac{1}{\tau} = -\frac{\partial S}{\partial P_1}$ was obtained at the thermodynamic equilibrium¹⁴⁻¹⁵, i.e.,

$$\tau = \frac{2}{\log(1 + P_1) - \log(1 - P_1)}. \quad [2]$$

This classical virtual temperature depends on the two-dimensional degree of polarization, which emphasizes that the system tends to evolve towards a higher polarization temperature state during multiple scattering.

In the quantum regime, the idea of virtual temperature was developed by assigning temperatures to pairs of energy levels (transitions) in a quantum system, which allowed the definition of virtual temperature as the ratio of the populations of the energy levels and their energy gap by using the Boltzmann factor⁶. For any object representing a pair (r, g) , where r is the actual mixed density matrix and g is the equilibrium density matrix, the virtual inverse temperature $\beta_{i,j}$ was defined as

$$\beta_{i,j} = \frac{\log\langle i|r|i\rangle - \log\langle j|r|j\rangle}{E_j - E_i}, \quad [3]$$

where $|i\rangle$ and $|j\rangle$ were the eigenstates of g with the corresponding energy eigenvalues E_i and E_j , respectively. The virtual temperature $T_{i,j}$ then was given by $T_{i,j} = \frac{1}{k_B \beta_{i,j}}$, k_B is the Boltzmann constant.

This framework allows us to determine the cooling potential of a resource: an object $O = (r, g)$ can effectively cool a qubit $Q = (s, s)$ with energy gap Δ and inverse temperature β if and only if there exists a pair of eigenvectors $|i\rangle$ and $|j\rangle$ of the Hamiltonian H such that

$$E_i - E_j = \Delta, \quad [4]$$

and

$$\beta_{i,j} > \beta. \quad [5]$$

This criterion exhibits the necessity of a specific relationship between the eigenstates and the energy levels for successful cooling. This concept was vital for understanding quantum thermodynamic systems, where a negative value of the virtual temperatures indicates the presence of population inversion.

Building on this foundation, several authors⁷⁻¹³ further explored the implications of virtual temperatures in quantum thermodynamics. They defined passive states as those where every transition has a positive virtual temperature and completely passive states where every transition has the same positive virtual temperature⁸. This extension provided a deeper understanding of the conditions under which work can be extracted from quantum systems. More recently, an operational definition of the virtual temperatures of a quantum state was proposed¹³. This definition considered virtual temperature a measurable quantity based on the similia construal of the Zeroth law of thermodynamics. This approach emphasizes measurable properties and practical implications, which offers a robust framework for understanding virtual temperature in quantum thermodynamics.

However, the framework for defining virtual temperature in these studies is constrained by assumptions of idealized conditions and the complexity of managing multi-level interactions while keeping a constant energy gap between the two levels¹¹. Furthermore, the impact of coherence and quantum correlations, which can significantly alter thermodynamic properties, is frequently overlooked. These limitations underscore the need for further research to refine these models, which may make them applicable by using a more rigorous approach. Additionally, exploring the interaction of virtual temperature with other thermodynamic quantities, processes, and relations, such as entropy, entropy production, and entropic uncertainty relations¹⁶⁻¹⁷, could provide a more comprehensive understanding of quantum thermal systems.

Here we explore a more generic and more natural interpretation of statistical virtual temperature using the spectrum of the Gibbs Kubo-Martin-Schwinger (KMS) state in terms of $d-1$ indices of purity (IP), where d represents the dimension of the Hilbert space in the C^* -algebra. We found that the universal physical bounds between the von Neumann entropy and statistical virtual temperature depend on the values of the IPs, which allow any point on these planes to be expressed as a convex combination of extreme points that may represent a classical or quantum separable state. These IPs give information on the physical phenomena in different scenarios considered in quantum and classical regimes such as bias in quantum thermal machines¹¹ and degree of polarization, degree of coherence, and degree of

directionality of an arbitrary classical electromagnetic field¹⁵. We further demonstrate the usefulness of these diagrams for the characterization and classification of the classical arbitrary polarization fields and in understanding the quantum Mpemba effect. Moreover, we rendered a geometric view of the third law of thermodynamics using these entropy-temperature diagrams. Nonetheless, the statistical virtual temperature we defined exhibits the third law of thermodynamics as discussed in a later section.

Results

Statistical Virtual Temperature

Consider a special class of the KMS state¹⁸, i.e., the Gibbs state ω_Λ with Hamiltonian H_Λ for a quasi-local quantum system as it allows us to extend the theory to the thermodynamic limit (volume $V \rightarrow \infty$, Energy $E \rightarrow \infty$ with N/V and E/V finite). This can be done by using the Hahn-Banach theorem which extends ω_Λ to a state ω_Λ^G on all of \mathfrak{A} of C^* -algebra. We begin by letting γ be the labeling of countable sites of a system possessing some additional structure such as $\gamma = \mathbb{Z}^d$, then $\mathcal{p}_f(\gamma)$ is the subset of all finite subsets of γ . Assume $\Lambda_d \in \mathcal{p}_f(\gamma)$ then $\mathfrak{A}(\Lambda_d)$ is a d -dimensional matrix C^* -algebra and is given as

$$\mathfrak{A}(\Lambda_d): = \bigotimes_{x \in \Lambda_d} M_d(\mathbb{C}). \quad [6]$$

Any state ω_{Λ_d} can be written on $\mathfrak{A}(\Lambda_d)$ in the form

$$\omega_{\Lambda_d}(A) = \text{tr}(\rho_{\Lambda_d} A) \quad [7]$$

for some d -dimensional density matrix ρ_{Λ_d} with tr standing trace, where the representation of $\mathfrak{A}(\Lambda_d)$ on the Hilbert space $\mathcal{H}_{\omega_{\Lambda_d}}$ is a $*$ -isomorphic and recovered through the Gelfand, Naimark, and Segal (GNS) construction. The state $\omega_{\Lambda_d}(A)$ is the KMS state that satisfies the relations,

$$F_{AB}(t) = \omega_{\Lambda_d}(A \alpha_t^\wedge(B)), \quad [8]$$

$$F_{AB}(t + i\hbar\beta) = \omega_{\Lambda_d}(\alpha_t^\wedge(B)A), \quad [9]$$

and the function F_{AB} is analytic on the interior of the strip $\zeta_\beta = \{Z \in \mathbb{C} \mid \text{Im}(Z) \in [0, \hbar\beta]\}$, where $t \in \mathbb{R}$ with A and B matrices in $M_d(\mathbb{C})$ are the elements of $\mathfrak{A}(\Lambda_d)$. The time automorphism is written as $\alpha_t^\wedge(A) = e^{itH_{\Lambda_d}} A e^{-itH_{\Lambda_d}}$. Thus, the von Neumann entropy for a quasi-local algebra for a C^* -dynamical system $(\mathfrak{A}, \alpha_t^\wedge)$ is given by¹⁹⁻²²

$$S_{\Lambda_d}(\omega) = -\text{tr}(\rho_{\Lambda_d} \log \rho_{\Lambda_d}). \quad [10]$$

It is worth mentioning here as that of the ensemblist view that the von Neumann entropy $S_{\Lambda_d}(\omega)$, describes the entropy of a quantum system, analogous to the Gibbs entropy, $S_G/k_B = -\int d\Gamma \rho(\Gamma) \log \rho(\Gamma)$, for classical system on the phase space Γ , where $\rho(\Gamma)$ is the probability density function²³⁻²⁴. Conversely, the individualists argue that the Boltzmann entropy is more suitable for quantum systems, given $S_B/k = \log(\dim \mathcal{H})$, $\dim \mathcal{H}$ is the Hilbert space dimension²⁵. However, at thermodynamic

equilibrium, both entropy approaches are valid within the microcanonical ensemble²⁵. The necessity of using the KMS state arises from its role in providing a proper thermodynamic limit, which is crucial for consistent definitions of statistical virtual temperature and other thermodynamic-like quantities. The KMS condition ensures equilibrium properties that make it indispensable for maintaining consistency across statistical interpretations of virtual temperature.

We define d -dimensional statistical virtual inverse temperature β_d by writing the entropy per unit volume,

$$S_d(\omega) = \lim_{\Lambda \rightarrow \infty} S_{\Lambda_d}(\omega)/|\Lambda_d|, \quad [11]$$

for a translational invariant state ω (using the Von Hove notation) in terms of the indices of purity (IP) and comparing it with the Gibbs entropy, which can be obtained from the partition function using the transfer matrix approach or Jordan-Wigner transformation²⁶⁻²⁷. Hence, we define the d -dimensional statistical inverse virtual temperature β_d ,

$$\beta_d = \frac{1}{u} \log_d \left[\frac{1+P_d}{1-P_d} \right], \quad [12]$$

where P_d is the d -dimensional degree of purity²⁸,

$$P_d = \sqrt{\frac{d[\text{tr}(\rho_{\Lambda_d}^2) - \text{tr}(\rho_{\Lambda_d})^2]}{d[\text{tr}(\rho_{\Lambda_d})^2] - \text{tr}(\rho_{\Lambda_d})^2}}, \quad [13]$$

with $u = a \left(\frac{e}{\pi}\right)^d$ (here $a \approx 2.671$), which is useful in the geometric description of the unattainability principle for classical and quantum thermodynamic systems. We assumed that the d -dimensional density matrix for the KMS state

$$\rho_{\Lambda_d} = \frac{e^{-\beta H_{\Lambda_d}}}{\text{tr}(e^{-\beta H_{\Lambda_d}})} \quad [14]$$

is a normalized state. The d -dimensional temperature $\tau_d \equiv \frac{1}{\beta_d}$, with $J = k_B = 1$ is invariant under change in the basis of ρ_{Λ_d} , that is

$$\tau_d(\rho_{\Lambda_d}) = \tau_d(U\rho_{\Lambda_d}U^\dagger). \quad [15]$$

The term P_d is over all purity measure of the system which can also be written in terms of the $d - 1$ IP given as²⁸

$$P_d = \sqrt{\frac{d}{d-1} \left(\sum_{k=1}^{d-1} \frac{P_{(k)}^2}{k(k+1)} \right)} \quad [16]$$

for $k = 1, 2, \dots, d - 1$. The k^{th} IP value is defined from the d eigenvalues λ_i ($i = 1, 2, \dots, d$) of ρ_{Λ_d} such that the generalized expression for the IP is²⁸

$$P_{(k)} = \sum_{i=0}^{k-1} \lambda_i - k\lambda_k, \quad [17]$$

which obeys the relation²⁸

$$0 \leq P_{(1)} \leq P_{(2)} \leq \dots \leq P_{(d-1)} \leq 1. \quad [18]$$

The k^{th} and the smallest eigenvalue of ρ_{Λ_d} in terms of the IP can be written as

$$\lambda_k = \left[\frac{1}{d} - \frac{P_{(k)}}{k+1} + \sum_{l=k+1}^{d-1} \frac{P_{(l)}}{l(l+1)} \right], \quad [19]$$

With $0 \leq k < d - 1$, with $P_{(0)} = 0$ and

$$\lambda_{d-1} = \left[\frac{1}{d} - \frac{P_{(d-1)}}{d} \right], \quad [20]$$

respectively²⁸. It is worth noting that the polarization temperature for the plane wave in Eq. (2) has been recovered from Eq. (12) by assuming $d = 2$ for the two-dimensional ρ_{Λ_2} . Additionally, as the overall measure of the statistical purity of the system is P_d , we may define the generalized expression for the overall purity as,

$$PI_d = \left| \sqrt{\frac{\sum_{k=1}^{d-1} P_{(k)}^2}{d-1}} \right|, \quad [21]$$

which can provide useful information on a classical or quantum system under study. Since PI_d is considered the overall purity measure with equal weight, if β_d were a function of PI_d , the entropy-temperature diagrams would provide information about the maximum and minimum disorder without showing further classification, unlike in the case of P_d .

Discussion

In this study, we introduced the concept of d -dimensional virtual temperature expressed in terms of the IPs, which applies to both classical and quantum systems. Several authors previously used the concept of virtual temperature to understand the role of temperature in classical and quantum systems. However, the temperature they defined usually demands an unreasonable assumption of a constant energy gap between two levels⁶⁻¹³ or is limited to the two-dimensional system⁵. The generalized expression Eq. (12) we provided is independent of these assumptions and applies to any generic quantum state that can be represented by the thermal Gibbs KMS state. Furthermore, we studied the universal physical bounds between entropy and temperature for d -dimensional classical and quantum systems and established that $d-1$ IPs can help us understand subtle classical and quantum phenomena such as classical polarization theory and quantum Mpemba effect.

One of the key results of this study is the geometric interpretation we provided for the Nernst unattainability principle. Conventionally, the Nernst principle suggests that absolute zero temperature is unattainable in finite steps, nevertheless, by interpreting this principle in terms of the dimensionality of the Hilbert space, we offered a new perspective on why this is the case. The dimensional structure of quantum systems imposes intrinsic limitations on the approach to absolute zero, which can be understood geometrically with the number of cusp points in the entropy-temperature diagrams. This geometric viewpoint not only reinforces the classical interpretation of the Nernst principle but also provides a novel lens through which we can analyze temperature and entropy in quantum systems. These findings highlight the importance of universal entropy-temperature bounds, as they impose fundamental constraints on the thermodynamic behavior of systems, both classical and quantum. Understanding these constraints can potentially open new avenues for exploring intricate phenomena, particularly in systems with complex quantum states. As such, the work presented here lays the groundwork for future research into how virtual temperature, entropy, and the underlying geometry of quantum systems are interrelated which may offer both a theoretical foundation and practical insights into the nature of classical and quantum systems.

Methods

We now utilize a Monte Carlo algorithm to generate a uniform distribution of points on a d -dimensional unit sphere, where each point's coordinates correspond to a valid set of IPs. This method enabled us to produce the entropy-temperature diagrams shown in Fig 1 (1-d).

Entropy-Temperature Diagrams

The entropy-temperature diagrams for d -dimensional ρ_{\wedge_d} are shown in Fig. 1 (a-d). These diagrams depict the connections between different stages of a generic quantum state, which may be characterized by the varying symmetries present in their density matrices or reduced density matrices in the case of quantum entanglement. The figures illustrate the entropy-temperature diagrams for density matrices of varying dimensions, specifically $d = 2, 3, 4$, and 9. These diagrams highlight the intricate relationships between the von Neumann entropy $S_d(\omega)$ (or S_d) and the statistical virtual temperature τ_d that are pivotal in understanding the quantum state's characteristics. The points and curves are generated by specific constraints on the values of the IPs²⁹⁻³⁰. Thus, one can use these entropy-temperature diagrams to characterize and classify the states and dynamics of an arbitrary quantum system.

The IPs for a given d -dimensional Hilbert space provide a quantitative measure of the eigenvalue distribution of the density matrix. For $d = 2$, the two eigenvalues are arranged in a form $\lambda_0 \geq \lambda_1$ give

$$P_{(1)} = \frac{\lambda_0 - \lambda_1}{\lambda_0 + \lambda_1} = \tanh(\beta_2). \quad [22]$$

Therefore, the entropy-temperature diagram is a curve as shown in Fig. 1. (a). Note that this is the degree of polarization when the system is a classical plane polarized light^{5, 15}, and it is the bias when the system under study is a quantum thermal machine¹¹. When we have a higher dimensional density matrix for a classical or quantum system, the entropy and temperature are multifunction of $d - 1$ IPs, which is shown in entropy-temperature diagrams in Fig. 1 (c-d). For instance, for $d = 4$, the indices of purity are expressed as follows²⁸,

$$P_{(1)} = \lambda_0 - \lambda_1, \quad [23]$$

$$P_{(2)} = \lambda_0 + \lambda_1 - 2\lambda_2, \quad [24]$$

$$P_{(3)} = \lambda_0 + \lambda_1 + \lambda_2 - 3\lambda_3, \quad [25]$$

with $\text{tr}(\rho_{\Lambda_d}) = 1$, thus, the feasible regions, curves, and cusp points are generated by the relation²⁸⁻³⁰,

$$0 \leq P_{(1)} \leq P_{(2)} \leq P_{(3)} \leq 1, \quad [26]$$

which is the consequence of the fact that the eigenvalues are arranged in the form^{15, 30},

$$\lambda_0 \geq \lambda_1 \geq \lambda_2 \geq \lambda_3. \quad [27]$$

These entropy-temperature diagrams thus serve as powerful tools for the characterization, quantification, and classification of the states and dynamics of arbitrary classical and quantum systems, which offers a detailed understanding of the various physical phenomena we discussed in the following.

Classical optical polarization theory

The theory of partial polarization employs the concepts of correlation functions and d -dimensional polarization matrix Φ_d , which are based on the statistical nature of the field components as analytic signals^{5, 14-15}. The complex analytic signal is considered at a point \mathbf{r} as a quasimonochromatic optical field of zero-mean variable with a Gaussian spectral profile, such that the second-order statistical moments are sufficient. The ergodicity of a stochastic stationary process is taken at least in the wide sense. The fluctuating electric vector is captured by the polarization density matrix which is written as,

$$\rho_{\Lambda_d} = \frac{\Phi_d}{\text{tr}(\Phi_d)} \quad [28]$$

with trace $\text{tr}(\Phi_d) = 1$. The ρ_{Λ_d} is non-negative definite and Hermitian. This matrix can be diagonalized to yield real, non-negative eigenvalues, and its expansion in terms of the $SU(d)$ Lie group gives rise to the normalized Stokes parameters $Y_j^{(d)}$. These parameters are defined by the scalar coefficients in the expansion of ρ_{Λ_d} using a number of d^2 Hermitian, trace orthogonal, and linearly independent matrices $O_j^{(d)}$. This framework fully characterizes the state of polarization of the optical field. Important features

include the normalization and orthogonality conditions of these matrices, with specific sets such as four Pauli matrices for $d = 2$, eight Gell-Mann matrices for $d = 3$, and the extended set of sixteen Dirac matrices for $d = 4$, representing plane and arbitrary polarization states and polarized light-matter interaction, respectively. The three-dimensional degree of purity, P_3 , serves as a measure of the degree of polarization of the optical field^{14-15, 31}.

Here we will employ our theory of entropy-temperature diagrams for the characterization and classification of a non-paraxial electromagnetic field with $d = 3$, using the statistical virtual temperature τ_3 and von Neumann polarization entropy S_3 . The cusp in Fig. 1(b) and the three curves are obtained by setting all possible constraints on the IP inequality,

$$0 \leq P_{(1)} \leq P_{(2)} \leq 1. \quad [29]$$

The cusp point A represents a plane unpolarized state whose polarization ellipse is completely random but remains fixed in a plane, i.e., $P_{(1)} = 0$ and $P_{(2)} = 1$ ($P_3 = 1/2$). The curve between point A (excluded) and points where $\tau_3 \rightarrow 0$ represents all the possible states with $P_3 > 1/2$, i.e., $P_{(2)} = 1$ and $0 < P_{(1)} \leq 1$. These states can be considered as incoherent compositions of the two polarization eigenstates of ρ_{Λ_d} with nonzero eigenvalues whose polarization planes are in general different¹⁵. In the limiting case that the polarization planes of both components coincide, the polarization state is called regular, otherwise, it is said to be nonregular³².

The curve extending from point A to the regions where $\tau_3 \rightarrow \infty$ corresponds to states with $P_3 < \frac{1}{2}$. These states have the first IP of zero, $P_{(1)} = 0$, which means that the two more significant eigenstates of the polarization matrix have equal weights. The second IP ranges from $0 \leq P_{(2)} \leq 1$ and with $P_{(2)} = 1$ at point A represents two-component states. As $P_{(2)}$ decreases (with $P_{(2)} < 1$), the state must contain three incoherent components, eventually reaching $P_{(2)} = 0$, thus, the state can be interpreted as an equiprobable incoherent mixture of the three eigenstates of the polarization matrix. Therefore, excluding point A , this curve contains both regular and nonregular three-component polarization states.

At this point it is worth recalling that the degree of nonregularity of a polarization state is determined by the properties of the characteristic decomposition of the polarization density matrix^{15,31}, given as

$$\rho_{\Lambda_{d3}} = P_{(1)}\rho_{3p} + (P_{(2)} - P_{(1)})\rho_{3m} + (1 - P_{(2)})\rho_{3u} \quad [30]$$

with $\text{tr}(\rho_{\Lambda_3}) = 1$. The pure component is expressed as $\rho_{3p} = (U \text{diag}(1,0,0) U^\dagger)$, where U is the unitary diagonalization matrix^{31, 33}. It contains only the single more significant (larger eigenvalue) polarization eigenstate of ρ_{Λ_3} . The middle component $\rho_{3m} = (1/2)(U \text{diag}(1,1,0) U^\dagger)$ is called the discriminating

component³⁴, which is prepared as an equiprobable mixture of the two eigenstates with major associated eigenvalues. The arbitrary wave unpolarized component is written as $\rho_{3u} = \left(\frac{1}{3}\right) (U\text{diag}(1,1,1)U^\dagger) = \left(\frac{1}{3}\right) I_3$ (I_3 , being the 3x3 identity matrix), which has an equally probable mixture of all the three eigenstates.

The matrix ρ_{3m} has always rank = 2, while the rank $m = \text{rank}(\text{Re}\rho_{3m})$ of its real part is limited by $2 \leq m \leq 3$, whose minimal value $m = \text{rank}(\rho_{3m}) = 2$ constitutes a genuine property of regular states³².

The upper curve with maximum entropy is obtained by setting $P_{(1)} = P_{(2)}$, hence, $\rho_{3m} = 0$ in the characteristic decomposition. Therefore, the curve only contains regular polarization states without a discriminating component, consequently, a point on the curve can always be decomposed into a fully polarized component ρ_{3p} and an unpolarized component ρ_{3u} . For all other possibilities of $P_{(1)} < P_{(2)} < 1$, the points are bounded by the three curves in which all three components are present in the characteristic decomposition.

Quantum phenomena: entanglement gradient and temperature-resolved entanglement asymmetry

On the entropy-temperature diagrams, along an isothermal (isentropic) curve, there can be many quantum states that have different entropies (temperature). We define two new quantities that can enhance our understanding of quantum phenomena using these universal entropy-temperature diagrams: the entropy gradient (or entanglement gradient),

$$E_g = \frac{\partial S_d}{\partial \tau_d}, \quad [31]$$

and temperature-resolved entanglement asymmetry $E_{S,i}$,

$$E_{S,i} = \left| \frac{S_{d,i,Q}}{\tau_{d,i,Q}} - \frac{S_{d,i}}{\tau_{d,i}} \right|, \quad [32]$$

where i belongs to a subsystem with subscript Q representing charge operator such that $[\rho_{\wedge,i}, Q] \neq 0$ ³⁵⁻³⁶. Entropies and temperatures can be obtained for the subsystem i and its projection on the eigen basis reduced density matrix i_Q of a composite system. When the entropies and temperatures corresponding to the reduced density matrices are located at the same point of the plane, representing a maximally mixed entangled state where knowledge of one subsystem provides no information about the other, then E_g provides further information about which state is more sensitive to the temperature variation. For instance, a higher value of E_g for the reduced matrices $\rho_{\wedge,A}$ and $\rho_{\wedge,B}$ of a bipartite system suggests that small changes in temperature can lead to large changes in entanglement. This could be particularly important for understanding how sensitive a quantum system is to thermal fluctuations. Furthermore,

any point on the cusp points where a sharp change in the entropy of the reduced density matrix with a small variation in the temperature range might indicate a transition from a separable to an entangled state, indicating a phase transition. On the other hand, if the points belonging to the subsystems of a bipartite composite system and their projectors representing $\rho_{\wedge,A}$, $\rho_{\wedge,A,Q}$ and $\rho_{\wedge,B}$, $\rho_{\wedge,B,Q}$ are different on the plane, then it suggests that the subsystems are not equally mixed, which often occurs in mixed states with varying degrees of decoherence due to different interactions with the environment.

To demonstrate the usefulness of the entropy-temperature diagram and the entanglement asymmetry span, we examine the effects of quantum decoherence and entanglement on a bipartite system initially prepared in a pure entangled state

$$|\psi_{AB}\rangle = \frac{1}{\sqrt{2}}(|00\rangle + |11\rangle), \quad [33]$$

The system's density matrix is

$$\rho_{\wedge,AB} = |\psi_{AB}\rangle\langle\psi_{AB}| = \frac{1}{2}(|00\rangle\langle 00| + |00\rangle\langle 11| + |11\rangle\langle 00| + |11\rangle\langle 11|), \quad [34]$$

with an entropy gradient of $E_g = 0$. Upon interaction with the environment and introducing a small perturbation $\varepsilon = 0.3$, subsystems undergo significant decoherence, resulting in the final mixed state

$$\rho_{\wedge,AB} = \frac{1}{4}(|00\rangle\langle 00| + |11\rangle\langle 11|) + \varepsilon(|00\rangle\langle 11| + |11\rangle\langle 00| + |01\rangle\langle 10| + |10\rangle\langle 01|) + \varepsilon^2(|01\rangle\langle 01| + |10\rangle\langle 10|), \quad [35]$$

and the reduced density matrices are

$$\rho_{\wedge,A} = \text{tr}_{\wedge,B}(\rho_{\wedge,AB}) = \rho_{\wedge,B} = \text{tr}_{\wedge,A}(\rho_{\wedge,AB}) = 0.5|0\rangle\langle 0| + 0.15|0\rangle\langle 1| + 0.15|1\rangle\langle 0| + 0.5|1\rangle\langle 1|, \quad [36]$$

with entropies and temperatures of the subsystems are $S_2(\rho_{\wedge,A}) = S_2(\rho_{\wedge,B}) = 0.934$ and $\tau_2(\rho_{\wedge,A}) = \tau_2(\rho_{\wedge,B}) = 3.2308$, respectively, while the whole system has entropy $S_4(\rho_{\wedge,A,B}) = 0.7040$ and temperature $\tau_4(\rho_{\wedge,A,B}) = 1.8768$ (see Fig. 2(a-b)). It is interesting to note that for $\varepsilon = 0.5$, the system remains in the entangled state while $\varepsilon > 0.5$ makes it a separable state. To determine $\rho_{\wedge,A,Q}$, we projected $\rho_{\wedge,A}$ onto eigenspaces of the charge operator Q_A resulting in

$$\rho_{\wedge,A,Q} = 0.5|0\rangle\langle 0| + 0.5|1\rangle\langle 1|, \quad [37]$$

with an entropy $S_2(\rho_{\wedge,A,Q}) = 1$ and temperature $\tau_2(\rho_{\wedge,A,Q}) \rightarrow \infty$. Consequently, the entanglement asymmetry $\Delta S_i = 0.0659$ (with $i = A, B$) indicates a small degree of symmetry breaking within the subsystems. However, the $E_{S,i} = 0.2891$ is significant enough to be detected experimentally. This implies that while ΔS_i points to a subtle asymmetry, $E_{S,i}$ is a more pronounced indicator and thus a better candidate for experimental observation. Hence, an experimenter can perform time sequential measurements starting with time $t = 0$ to $t = t_M$, t_M being the Mpemba time that satisfy the condition

$$E_{S,A,i}(0) - E_{S,A,j}(0) < 0, \quad [38]$$

($i, j = 1, 2$ are two systems) and subsequently the relation

$$E_{S,A,i}(t) - E_{S,A,2}(t) < 0 \text{ for } \forall t > t_M, \quad [39]$$

to observe the pattern on the entropy-temperature diagram that may help understand the intricate phenomena of the Mpemba effect for a quantum system³⁶.

Geometric view of the third law of thermodynamics

The statistical inverse temperature β_d , we defined from the d -dimensional density matrix ρ_{Λ_d} , exhibits the phenomenon of the unattainability of absolute zero temperature. This is the manifestation of the most accepted form of the third law of thermodynamics, i.e., $\beta_d \rightarrow \infty$ when $P_d = 1$, which shows the unattainability of an irreducible Hilbert space $\mathcal{H}_{\omega_\Lambda}$ representing a completely pure state. This asymptotic behavior shows that creating a completely polarized and perfectly pure quantum state in a laboratory is impossible or such states do not exist in nature. Fig. 3 (a-b) shows the behavior of the β_d for two and three-level systems ($d = 2, 3$) when $P_d \rightarrow 1$. Several authors have recently used quantum resource theories to interpret and quantify the third law of thermodynamics³⁷⁻³⁹, for example, theorems for the limitation of the purification of resources for a full-ranked density matrix were stated³⁷ and the derivation for the unattainability of absolute zero temperature was determined³⁸. Their work implies that the set of ground KMS states that generate any strictly local and bounded interaction φ at inverse KMS temperature $\beta = \infty$ is impossible. However, there has been criticism of the common assumption that ground states of quantum systems are always unique and that the set is non-empty⁴⁰. It was pointed out that these researchers avoid making this assumption⁴¹.

Here, we employ the geometric approach to describe the third law of thermodynamics. We know that the Nernst unattainability principle applies to both classical and quantum systems and is related to the requirement of an infinite-dimensional Hilbert space. The entropy per unit volume defined on a quasi-local algebra d -dimensional matrix algebra

$$S_d(\omega) = - \left\{ \sum_{k=0}^{d-1} \left(\left[\frac{1}{d} - \frac{P(k)}{k+1} + \sum_{l=k+1}^{d-1} \frac{P(l)}{l(l+1)} \right] \log_d \left[\frac{1}{d} - \frac{P(k)}{k+1} + \sum_{l=k+1}^{d-1} \frac{P(l)}{l(l+1)} \right] \right) \right\} - \left[\frac{1}{d} - \frac{P_{d-1}}{d} \right] \log_d \left[\frac{1}{d} - \frac{P_{d-1}}{d} \right], \quad [40]$$

with $P_{(0)} = 0$ goes to a minimum value of zero and the inverse temperature

$$\beta_d = \frac{1}{u} \log_d \left[\frac{1 + \sqrt{\frac{d}{d-1} \left(\sum_{k=1}^{d-1} \frac{P(k)^2}{k(k+1)} \right)}}{1 - \sqrt{\frac{d}{d-1} \left(\sum_{k=1}^{d-1} \frac{P(k)^2}{k(k+1)} \right)}} \right] \quad [41]$$

reaches infinity (or $\tau_d \rightarrow 0$) on the entropy-temperature diagram. A complete pure classical or quantum state has $\tau_d = 0$, if and only if $P_1 = 1$. Thus, we need infinite resources to produce a pure classical state or to cool any quantum state to the point corresponding to the IPs values

$$P_{(1)} = P_{(2)} = \dots = P_{(d-1)} = 1, \quad [42]$$

with $d \rightarrow \infty$. Consequently, any purification or distillation needs to go through an infinite number of cusp points on the plane. This can be seen inevitably from the definition of the statistical inverse temperature with $u = a \left(\frac{e}{\pi}\right)^d \rightarrow 0$ when $d \rightarrow \infty$, thus $\beta_d \rightarrow \infty$, representing a pure state.

Code availability

The computer codes used to produce the results presented in this paper are available from the authors upon reasonable request.

Reference

1. Hartmann, M., Mahler, G. & Hess, O. Existence of temperature on the nanoscale. *Phys. Rev. Lett.* **93**, 080402 (2004).
2. Hsiang, J. T. & Hu, B. L. Nonequilibrium quantum free energy and effective temperature, generating functional, and influence action. *Phys. Rev. D* **103**, 065001 (2021).
3. Kliesch, M., Gogolin, C., Kastoryano, M. J., Riera, A. & Eisert, J. Locality of temperature. *Phys. Rev. X* **4**, 031019 (2014).
4. Mitchison, M. T., Purkayastha, A., Brenes, M., Silva, A. & Goold, J. Taking the temperature of a pure quantum state. *Phys. Rev. A* **105**, L030201 (2022).
5. Brosseau, C. & Bicut, D. Entropy production in multiple scattering of light by a spatially random medium. *Phys. Rev. E* **50**, 4997 (1994).
6. Janzing, D., Wocjan, P., Zeier, R., Geiss, R. & Beth, T. Thermodynamic cost of reliability and low temperatures: Tightening Landauer's principle and the second law. *Int. J. Theor. Phys.* **39**, 2717–2753 (2000).
7. Quan, H. T., Liu, Y.-x., Sun, C. P. & Nori, F. Quantum thermodynamic cycles and quantum heat engines. *Phys. Rev. E* **76**, 031105 (2007).
8. Skrzypczyk, P., Silva, R. & Brunner, N. Passivity, complete passivity, and virtual temperatures. *Phys. Rev. E* **91**, 052133 (2015).
9. Mitchison, M. T. Quantum thermal absorption machines: refrigerators, engines and clocks. *Contemp. Phys.* **60**, 164–187 (2019).

10. Brunner, N., Linden, N., Popescu, S. & Skrzypczyk, P. Virtual qubits, virtual temperatures, and the foundations of thermodynamics. *Phys. Rev. E* **85**, 051117 (2012).
11. Silva, R., Manzano, G., Skrzypczyk, P. & Brunner, N. Performance of autonomous quantum thermal machines: Hilbert space dimension as a thermodynamical resource. *Phys. Rev. E* **94**, 032120 (2016).
12. Koukoulekidis, N., Alexander, R., Hebdige, T. & Jennings, D. The geometry of passivity for quantum systems and a novel elementary derivation of the Gibbs state. *Quantum* **5**, 411 (2021).
13. Lipka-Bartosik, P., Perarnau-Llobet, M. & Brunner, N. Operational definition of the temperature of a quantum state. *Phys. Rev. Lett.* **130**, 040401 (2023).
14. Brosseau, C. *Fundamentals of Polarized Light: A Statistical Approach*. John Wiley, New York (1998).
15. Gil, J. J. & Ossikovski, R. *Polarized Light and the Mueller Matrix Approach*. CRC Press, Boca Raton (2022).
16. Wu, L., Ye, L. & Wang, D. Tighter generalized entropic uncertainty relations in multipartite systems. *Phys. Rev. A* **106**, 062219 (2022).
17. Wang, T. Y. & Wang, D. Entropic uncertainty relations in Schwarzschild space-time. *Phys. Lett. B* **855**, 138876 (2024).
18. Kubo, R. Statistical-mechanical theory of irreversible processes. I. General theory and simple applications to magnetic and conduction problems. *J. Phys. Soc. Japan* **12**, 570–586 (1957).
19. Kadanoff, L. P. *Quantum Statistical Mechanics*. CRC Press (2018).
20. Arveson, W. *An Invitation to C-Algebras**. Springer Science & Business Media (2012).
21. Bru, J. B. & de Siqueira Pedra, W. A. *C-Algebras and Mathematical Foundations of Quantum Statistical Mechanics: An Introduction**. Springer Nature (2023).
22. Bratteli, O. & Robinson, D. W. *Operator Algebras and Quantum Statistical Mechanics I*. Texts and Monographs in Physics, 2nd edn, Springer, Berlin (1997).
23. Campisi, M. Construction of microcanonical entropy on thermodynamic pillars. *Phys. Rev. E* **91**, 052147 (2015).
24. Hilbert, S., Hänggi, P. & Dunkel, J. Thermodynamic laws in isolated systems. *Phys. Rev. E* **90**, 062116 (2014).
25. Goldstein, S., Lebowitz, J. L., Tumulka, R. & Zanghì, N. Gibbs and Boltzmann entropy in classical and quantum mechanics. In *Statistical Mechanics and Scientific Explanation: Determinism, Indeterminism and Laws of Nature* 519–581 (2020).
26. Ohya, M. & Petz, D. *Quantum Entropy and Its Use*. Springer Science & Business Media (2004).

27. Jordan, P. & Wigner, E. P. Über das Paulische Äquivalenzverbot. In *Springer Berlin Heidelberg* 109–129 (1993).
28. San José, I. & Gil, J. J. Invariant indices of polarimetric purity: Generalized indices of purity for $n \times n$ covariance matrices. *Opt. Commun.* **284**, 38–47 (2011).
29. Tariq, A., Li, P., Chen, D., Lv, D. & Ma, H. Physically realizable space for the purity-depolarization plane for polarized light scattering media. *Phys. Rev. Lett.* **119**, 033202 (2017).
30. Tariq, A., He, H., Li, P. & Ma, H. Purity-depolarization relations and the components of purity of a Mueller matrix. *Opt. Express* **27**, 22645–22662 (2019).
31. Gil, J. J., Friberg, A. T., Setälä, T. & San José, I. Structure of polarimetric purity of three-dimensional polarization states. *Phys. Rev. A* **95**, 053856 (2017).
32. Gil, J. J., Norrman, A., Friberg, A. T. & Setälä, T. Nonregularity of three-dimensional polarization states. *Opt. Lett.* **43**, 4611–4614 (2018).
33. Gil, J. J., Norrman, A., Friberg, A. T. & Setälä, T. Discriminating states of polarization. *Photonics* **10**, 1050 (2023).
34. Gil, J. J., Norrman, A., Friberg, A. T. & Setälä, T. Descriptors of dimensionality for $n \times n$ density matrices. *Eur. Phys. J. Plus* **138**, 1–7 (2023).
35. Ares, F., Murciano, S. & Calabrese, P. Entanglement asymmetry as a probe of symmetry breaking. *Nat. Commun.* **14**, 2036 (2023).
36. Rylands, C., Klobas, K., Ares, F., Calabrese, P., Murciano, S. & Bertini, B. Microscopic origin of the quantum Mpemba effect in integrable systems. *Phys. Rev. Lett.* **133**, 010401 (2024).
37. Fang, K. & Liu, Z. W. No-go theorems for quantum resource purification. *Phys. Rev. Lett.* **125**, 060405 (2020).
38. Masanes, L. & Oppenheim, J. A general derivation and quantification of the third law of thermodynamics. *Nat. Commun.* **8**, 1 (2017).
39. Buffoni, L., Gherardini, S., Cruzeiro, E. Z. & Omar, Y. Third law of thermodynamics and the scaling of quantum computers. *Phys. Rev. Lett.* **129**, 150602 (2022).
40. Naaijken, P. *Quantum Spin Systems on Infinite Lattices: A Concise Introduction*. Lecture Notes in Physics, Springer (2017).
41. Uffink, J. Masanes and Oppenheim on the third law of thermodynamics. *Found. Phys.* **47**, 871–872 (2017).

Acknowledgment

This work was supported by the National Natural Science Foundation of China (Grant Nos. 12475009, 12075001, and 61601002), Anhui Provincial Key Research and Development Plan (Grant No. 2022b13020004), Anhui Province Science and Technology Innovation Project (Grant No. 202423r06050004), and Anhui Provincial University Scientific Research Major Project (Grant No. 2024AH040008).

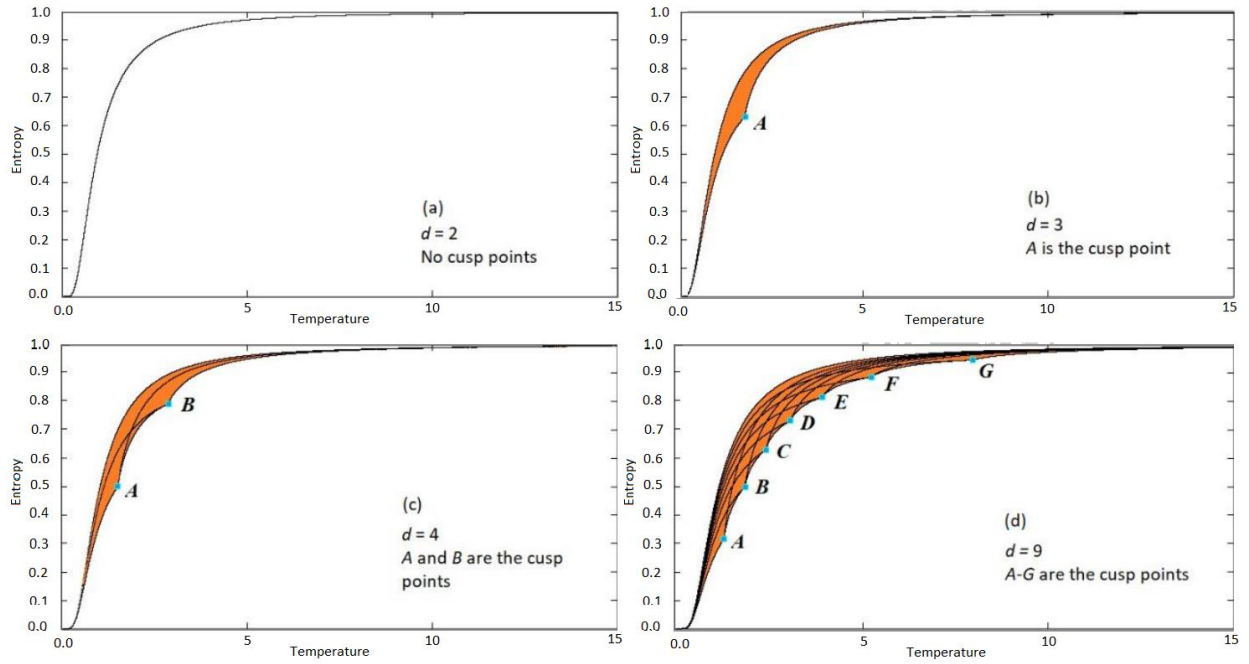


Figure 1(a-d): Entropy-temperature diagrams for d -dimensional density matrices (or reduced density matrices) for $d=2,3,4$, and 9. The orange shades are physically realizable regions separated by black curves which are generated by limiting IP values and the blue A to G are the cusp points. The $d-2$ cusp points may indicate quantum phase transitions at critical points which may be explored for some physical models in future studies.

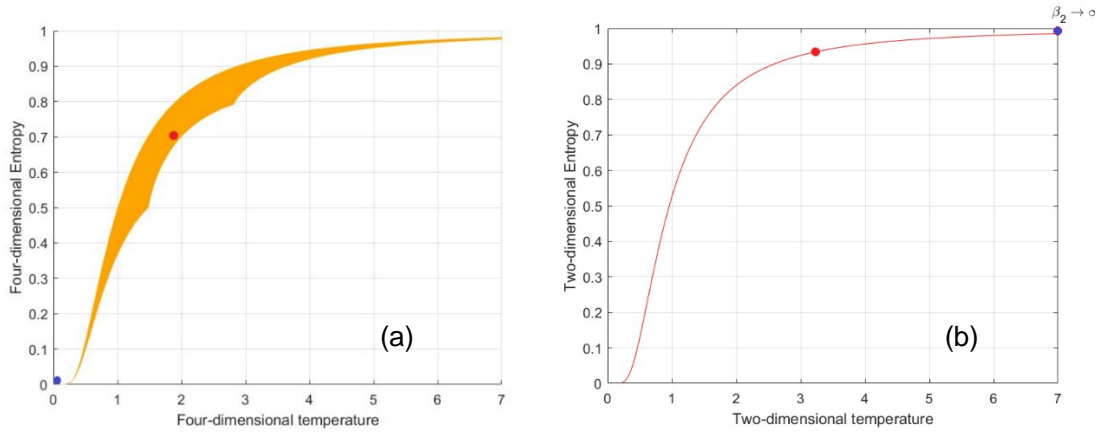


Figure 2(a-b): (a) The illustration of quantum decoherence for a pure Bell state that is shown with the blue dot while the red dot represents the decohered state. In (b), the entropy-temperature diagram for the reduced density matrices of a bipartite system (a) is shown. The red dot in (b) is the reduced density matrix of subsystem A (also B) and the blue dot shows that the projected reduced density matrix is located at infinity when the inverse temperature goes zero.

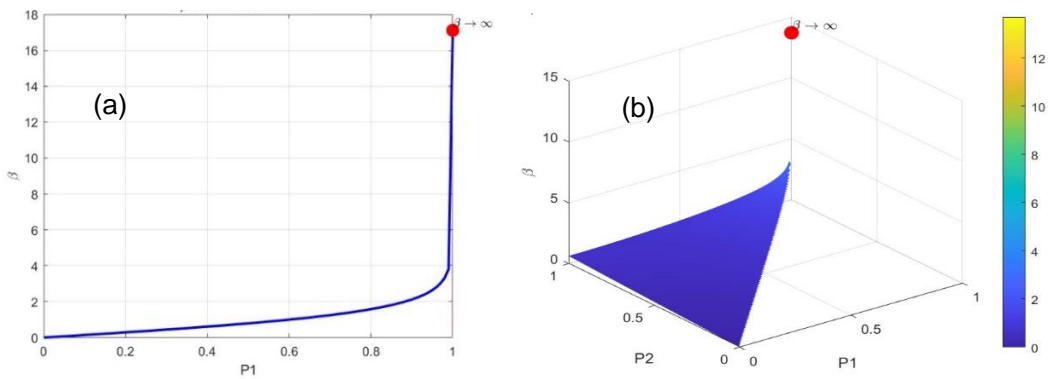


Figure 3(a-b): (a) The dependence of inverse temperature for (a) two-dimensional density matrix and (b) three-dimensional density matrix. Note that $P_{(1)} \leq P_{(2)}$ in (b).